RSC Advances

PAPER

View Article Online
View Journal | View Issue

Check for updates

Cite this: *RSC Adv.*, 2025, **15**, 33536

Inner-wall biochar-coated pipette tip microextraction for rapid and sustainable determination of tyrosine kinase inhibitors in plasma

Xiaofei Zhang,[a] Mengyuan Lv,[b] Yuyang Wang,[b] Nan Zhang*[b] and Di Chen *[b]

Tyrosine kinase inhibitors (TKIs) are critical in cancer therapy, but their clinical application is complicated by narrow therapeutic windows and significant interpatient variability in pharmacokinetics. To address this, this study presents an effective pipette-tip solid-phase microextraction (PT-μSPE) method using kapok fiber-derived biochar (KFB) as a green and cost-effective sorbent for the extraction of TKIs in plasma. The KFB was incorporated as an inner-wall coating within a standard pipette tip, minimizing backpressure and enhancing automation compatibility. This PT-μSPE method is optimized for efficiency and sensitivity, with ethanol used as the desorption solvent. The method is coupled with liquid chromatography-tandem mass spectrometry (LC-MS/MS) for the determination of TKIs, demonstrating excellent linearity (R^2 > 0.99), sensitivity (LOD: 0.022–0.125 ng mL^{-1}), and reproducibility. Furthermore, the method exhibits notable green chemistry characteristics, including minimal solvent usage and environmental sustainability. The proposed method offers a practical, scalable solution for TKI quantification for potential clinical and pharmacokinetic studies, with potential for high-throughput integration into automated systems.

Received 25th July 2025
Accepted 9th September 2025

DOI: 10.1039/d5ra05405b

rsc.li/rsc-advances

Open Access Article. Published on 15 September 2025. Downloaded on 1/19/2026 5:07:36 PM.
This article is licensed under a Creative Commons Attribution-NonCommercial 3.0 Unported Licence.

1. Introduction

Tyrosine kinase inhibitors (TKIs) are widely utilized in oncology for their selective suppression of intracellular kinase pathways that drive cancer cell growth and survival.[1,2] Despite their clinical utility, several TKIs exhibit narrow therapeutic windows and considerable interpatient pharmacokinetic variability, primarily attributable to cytochrome P450-mediated metabolism and interactions with other drugs or dietary components.[3,4] For example, Noda *et al.* reported that lenvatinib demonstrates a narrow therapeutic window, with effective plasma concentrations typically ranging from 70 to 290 ng mL^{-1}, while levels exceeding 300 ng mL^{-1} have been associated with increased risk of adverse effects such as hypertension and hepatic toxicity.[5] These factors complicate dosing strategies and increase the risk of subtherapeutic exposure or toxic accumulation, ultimately compromising therapeutic efficacy and safety.[6,7] In this context, therapeutic drug monitoring (TDM) plays a critical role in personalizing treatment regimens by ensuring that plasma drug concentrations remain within the optimal therapeutic range.

Currently, liquid chromatography-tandem mass spectrometry (LC-MS/MS) remains the method of choice for quantifying TKIs in plasma owing to its high sensitivity, selectivity, and capability for multiplexed analysis.[8,9] However, direct analysis of biological matrices remains challenging, primarily due to matrix effects that lead to signal suppression and reduced detection sensitivity.[10,11] Therefore, effective sample preparation is indispensable for minimizing matrix interferences, enriching target analytes, and improving analytical accuracy and precision. Among existing sample pretreatment strategies, pipette-tip micro-solid phase extraction (PT-μSPE) has gained increasing attention due to its simplicity, low solvent consumption, and compatibility with automation.[12,13] In this technique, the selection of an appropriate sorbent and sorbent-loading format is key to achieving high extraction efficiency and low backpressure—an essential factor for seamless integration with electronic pipetting systems. Although various materials such as electrospun fibers,[14,15] carbon-based sorbents,[16] and monoliths[17,18] have been explored, many suffer from limitations including high cost, complex fabrication, or incompatibility with automated systems due to inherent backpressure. To overcome these limitations and improve the practicality of PT-μSPE, increasing attention has been directed toward developing novel sorbents and loading formats that are not only efficient and cost-effective but also compatible with automated systems.

[a]*Department of Oncology, First Affiliated Hospital of Zhengzhou University, Zhengzhou 450052, China*
[b]*School of Pharmaceutical Sciences, Zhengzhou University, Zhengzhou 450001, China. E-mail: dichen@zzu.edu.cn; zhangnan@zzu.edu.cn*

© 2025 The Author(s). Published by the Royal Society of Chemistry

Open Access Article. Published on 15 September 2025. Downloaded on 1/19/2026 5:07:36 PM.
This article is licensed under a Creative Commons Attribution-NonCommercial 3.0 Unported Licence.

Natural plant-derived biochar presents a promising alternative due to its sustainability, low cost, and ease of preparation.[19] These materials not only offer environmental benefits but also possess tunable surface properties, making them well-suited for adsorption-based extraction techniques. Several studies have investigated various types of biochar, such as those derived from peanut shells-derived biochar,[20,21] corn cob-derived biochar,[22] banana-based biochar,[23] for use in PT-μSPE to achieve efficient extraction. However, these methods typically involve packing fine biochar powders into pipette tips using cotton plugs or mesh screens.[16,24] The small particle size often leads to increased flow resistance during liquid handling, which can reduce operational robustness and hinder compatibility with automated systems. Therefore, innovative strategies for the configuration and application of biochar-based sorbents are essential to fully exploit their potential in PT-μSPE.

Herein, an efficient PT-μSPE method was developed using kapok fiber-derived biochar (KFB) as a green, low-cost sorbent for selectively extracting TKIs from plasma. Kapok fiber, a naturally abundant biomass rich in cellulose and lignin, possesses a hollow tubular structure, low density, and high surface area.[25,26] Upon pyrolysis under oxygen-deprived conditions, these intrinsic features are translated into a porous biochar framework with abundant functional groups, providing favorable sites for hydrophobic and complementary polar interactions and facilitating rapid mass transfer. To address the common limitations associated with the use of fine biochar powders—such as elevated backpressure and poor automation compatibility—the KFB was innovatively immobilized as a uniform inner-wall coating within a standard pipette tip. This configuration enabled rapid, reproducible, and low-resistance solution handling, fully compatible with electronic pipetting systems. The developed KFB-PT-μSPE method was systematically optimized and evaluated in combination with LC-MS/MS for sensitively determining TKIs in plasma, with an emphasis on analytical performance, automation feasibility, and environmental sustainability. This approach demonstrates a practical, scalable solution for integrating natural-material-based sorbents into modern bioanalytical workflows.

2. Materials and methods

2.1. Chemicals and reagents

Methanol (MeOH), acetonitrile (ACN), and formic acid (FA), all of LC-MS grade, were sourced from Thermo Fisher Scientific Co., Ltd (MA, USA). Ethanol (EtOH) and acetone (AC) were purchase from sigma. Ultrapure water (H_2O) was generated using a Milli-Q system (Millipore, MA, USA). TKI reference standards were acquired from three vendors: ceritinib (Cer) from Bide Pharmatech Co., Ltd (Shanghai, China); erlotinib (Erl), ibrutinib (Ibru), pazopanib (Paz), nilotinib (Nilo), dasatinib (Dasa), and sunitinib (Suni) from Aladdin Biochemical Technology Co., Ltd (Shanghai, China); and imatinib (Ima) and gefitinib (Gef) from Shanghai Yien Chemical Technology Co., Ltd (Shanghai, China). Cyproconazole, used as the internal standard, was obtained from Shanghai Yien Chemical Technology Co., Ltd (Shanghai, China). Reagents used for phosphate buffer preparation—including dimethyl sulfoxide (DMSO), phosphoric acid (H_3PO_4), sodium hydroxide (NaOH), sodium dihydrogen phosphate (NaH_2PO_4), and disodium hydrogen phosphate (Na_2HPO_4)—were all sourced from Aladdin Reagent Co., Ltd (Shanghai, China). The molecular information and chemical structures of the studied TKIs—including their names, abbreviations, molecular formulas, molecular weights, Log *P* values, pK_a values and structures—are listed in Table S1.

Stock solutions (1 mg mL^{-1}) of each TKI and the internal standard were prepared in DMSO. All stock solutions were kept at −20 °C in the absence of light. A combined TKI working solution (10 μg mL^{-1} in ACN) was freshly prepared each week and maintained at 4 °C until use. Prior to use, the 10 μg mL^{-1} TKI mixture was subsequently diluted with water to prepare working concentrations for method optimization. A series of phosphate buffer solutions (PBS) with different pH values were prepared by adjusting the ratio of NaH_2PO_4 and Na_2HPO_4, followed by fine-tuning with either H_3PO_4 or NaOH as needed. All buffer solutions were freshly prepared and adjusted to the desired pH using a calibrated pH meter (PHS-3C, Leici Co., Ltd, Shanghai, China).

2.2. Plasma sample pretreatment

Residual blood collected during regular checkups from healthy individuals (25–40 years old) was used to prepare blank plasma samples. All volunteers had not received any medications, particularly the targeted TKIs. Specifically, blood samples were collected *via* venipuncture into heparinized tubes, followed by centrifugation at 5000×*g* for 10 min at 4 °C. The resulting plasma was stored at −80 °C in the dark for no longer than 3 months.

Plasma samples were thawed to ∼25 °C before use. Spiking was performed by adding defined volumes of TKI solutions and thoroughly mixing to achieve the desired concentrations. For each sample, 100 μL of blank plasma was combined with 5 μL of TKI solution and thoroughly vortexed to ensure homogeneity. To control the solution pH and dilute the plasma to reduce matrix effects, PBS (10 mM, pH 7.0) was added to adjust the pH and dilute the plasma to a final volume of 1 mL. The resulting solution was then subjected to subsequent extraction and analysis.

All experiments were performed in accordance with the Guidelines of the Declaration of Helsinki and relevant national regulations, and approved by the Ethics Committee of Zhengzhou University. Informed consents were obtained from all human participants involved in this study.

2.3. KFB-tip extraction procedure

The KFB was prepared by first pre-drying the fibers at 60 °C under vacuum overnight (∼24 h) to minimize moisture-related variability. The dried fibers were then carbonized in a tubular furnace under a continuous nitrogen flow (60 mL min^{-1}). The temperature was increased at a rate of 10 °C min^{-1} to 600 °C, maintained for 2 h to ensure thorough carbonization, and then naturally cooled to room temperature (∼25 °C) under nitrogen

Open Access Article. Published on 15 September 2025. Downloaded on 1/19/2026 5:07:36 PM.
This article is licensed under a Creative Commons Attribution-NonCommercial 3.0 Unported Licence.

protection. The resulting carbonized material was subsequently ground into a fine powder for use (Fig. S1).

To fabricate the KFB-tip device, approximately 50 μL of HT-902T silicone-based adhesive (Shanghai Huitian New Chemical Materials Co., Ltd, Shanghai, China) was aspirated into a 200 μL pipette tip, and the excess adhesive was removed by low-speed centrifugation (HL-4K mini palm centrifuge, Shanghai Huxi, China) at 4000 rpm for 1 min, forming a thin, uniform coating along the inner wall. An excess amount of KFB powder was then added into the tip, where it adhered to the adhesive-coated surface. The tip was left undisturbed at room temperature (~24 h) to allow the adhesive to fully cure. After curing, loosely bound particles were removed by centrifugation at 4000 rpm for 3 min, leaving only a firmly adhered thin coating along the channel wall (a schematic of the fabrication process is shown in Fig. S2A, and a photograph of the final KFB-tip is provided in Fig. S2B). Subsequently, the front end of a 1 mL pipette tip was trimmed and tightly connected to the KFB-coated tip to form a hollow extraction unit, which was then mounted onto an automated electronic pipette (dPette+, DLAB Scientific Co., Ltd, Beijing, China) (Fig. S3).

The procedure consisted of three main steps (Fig. 1A): sample loading, washing, and elution. Initially, the diluted sample solution (1 mL) was aspirated/dispensed through the KFB-tip for six cycles to ensure sufficient interaction between the TKIs and the KFB coating the inner surface of the tip. During this step, the target TKIs were selectively retained on the KFB, while matrix components were largely excluded. Subsequently, the tip was rinsed with 200 μL of H_2O, aspirated and dispensed twice, to remove any loosely bound impurities and reduce background interference. Finally, the retained TKIs were eluted by aspirating and dispensing 200 μL of EtOH over six cycles. The organic solvent disrupted TKI–sorbent interactions, facilitating effective elution. The resulting eluate was collected and directly subjected to subsequent LC-MS/MS analysis (Fig. 1B).

Due to their low cost and the high accuracy required in biological sample analysis, the KFB-coated tips were designed for single use to prevent potential carryover and ensure consistent performance.

2.4. LC-MS/MS analysis

LC-MS/MS analysis was performed using a Shimadzu Prominence LC system (Kyoto, Japan) coupled with an API 5500 triple quadrupole mass spectrometer equipped with a Turbo V™ electrospray ionization (ESI) source (AB Sciex, Framingham, MA, USA). Chromatographic separation was achieved on a Waters Acquity UPLC® BEH C18 column (50 mm × 2.1 mm, 1.7 μm; Milford, MA, USA). The mobile phases consisted of 0.1% FA in water (solvent A) and 0.1% FA in ACN (solvent B), delivered at a flow rate of 0.2 mL min^{-1} with an injection volume of 2 μL. The gradient elution was programmed as follows: starting with 5% B (0–0.15 min), ramped to 30% B at 0.2 min and held until 4.5 min, then increased to 60% B at 4.6 min and maintained until 7.0 min. The mobile phase was then returned to the initial condition (5% B) at 7.1 min and re-equilibrated for 2.9 min, yielding a total run time of 10 min.

Mass spectrometric detection was conducted in positive mode using multiple reaction monitoring (MRM). The ion spray voltage was maintained at 5500 V, while the source temperature was held at 550 °C throughout the analysis. Nitrogen was used as the nebulizer and auxiliary gas: curtain gas at 30 psi, Gas 1 (nebulizer gas) at 50 psi, and Gas 2 (heater gas) at 50 psi. The declustering potential, entrance potential, collision energy, and

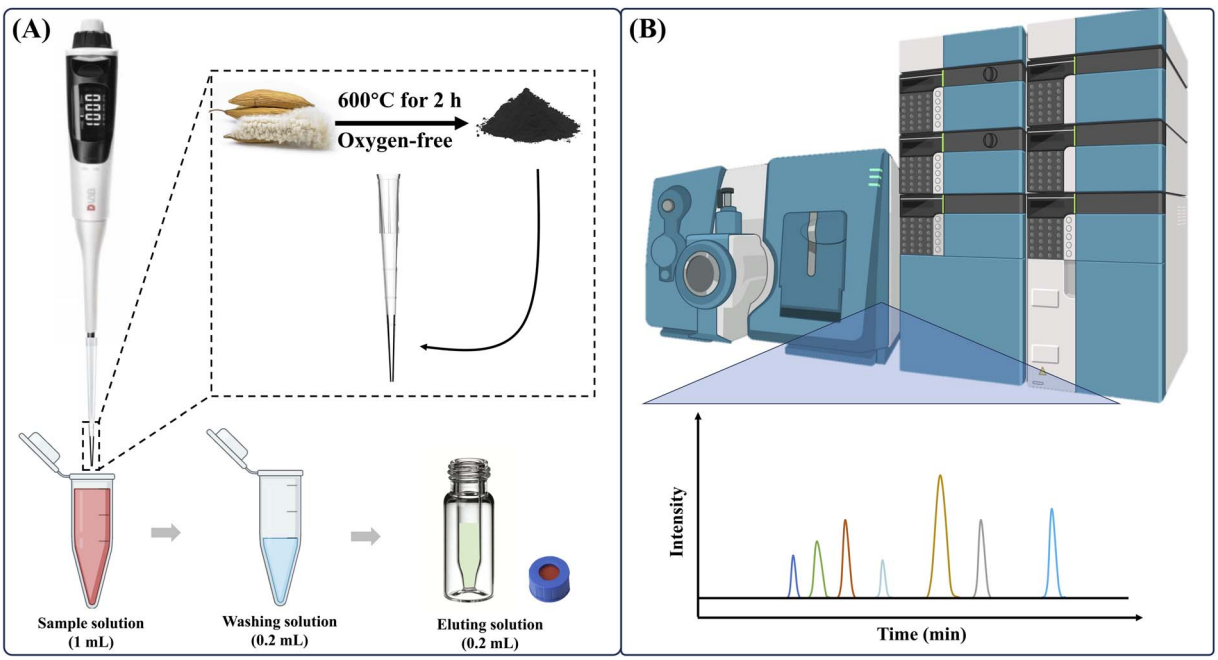

Fig. 1 Schematic illustration of (A) the KFB-tip-based PT-μSPE procedure and (B) subsequent direct LC-MS/MS analysis of the eluate.

© 2025 The Author(s). Published by the Royal Society of Chemistry

Open Access Article. Published on 15 September 2025. Downloaded on 1/19/2026 5:07:36 PM.
This article is licensed under a Creative Commons Attribution-NonCommercial 3.0 Unported Licence.

collision cell exit potential were optimized individually for each TKI, and the dwell time for each transition was set to 70 ms. All data acquisition and instrument control were performed using Analyst® software version 1.6.2 (AB Sciex). The optimized MRM transitions and associated parameters for each analyte are listed in SI Table S2.

3. Results and discussion

3.1. Characterization of KFB

The morphology and surface structure of the KFB were examined by scanning electron microscopy (SEM). As shown in Fig. 2, the KFB exhibited an irregular lamellar and fragmented morphology with a rough surface, which facilitates high surface contact during adsorption. The layered microstructure suggests the formation of abundant exposed edges and potential adsorption sites.

Textural properties of KFB were determined by N_2 adsorption–desorption isotherms at 77 K using a Micromeritics ASAP 2420 analyzer after degassing at 200 °C for 6 h; BET surface area was calculated in the P/P_0 range of 0.05–0.30, and pore size distribution was obtained by the BJH method. As shown in Fig. 3A, the isotherm displayed a typical type IV profile with a pronounced hysteresis loop, indicating suggesting high porosity. The Brunauer–Emmett–Teller (BET) surface area was calculated to be 374 $m^2\ g^{-1}$, highlighting the material's high porosity. The corresponding BJH pore size distribution curve (Fig. 3B) revealed a dominant pore diameter below 10 nm, confirming a mesoporous network. This porous architecture, combined with the high surface area, is advantageous for the adsorption and enrichment of small molecule analytes such as TKIs.

The surface chemistry of KFB was first analyzed by Fourier Transform Infrared Spectroscopy (FTIR). As shown in Fig. S4, the broad band around 3430 cm^{-1} originates from hydroxyl stretching vibrations, while the band at 1700 cm^{-1} is associated with carbonyl groups. The peaks at 1560 and 1350 cm^{-1} correspond to aromatic skeletal vibrations, and the absorption near 1150 cm^{-1} is attributed to C–O stretching. In addition, the signal around 600 cm^{-1} arises from out-of-plane bending vibrations. The presence of these polar functional groups increases the material's wettability toward aqueous solutions, thereby improving interfacial interactions and promoting the efficient extraction of analytes from aqueous samples.

X-ray photoelectron spectroscopy (XPS) further confirmed the surface elemental composition and bonding states of KFB. As shown in Fig. S5A, the survey spectrum revealed the presence of C 1s, O 1s, and N 1s peaks. The high-resolution C 1s spectrum (Fig. S5B) was deconvoluted into three components at approximately 284.8 eV (C–C), 285.8 eV (C–O), and 288.8 eV (C═O), accounting for 57.17%, 23.97%, and 18.86% of the total carbon signal, respectively. The predominance of C–C bonds indicates that KFB is primarily composed of a stable carbonaceous framework. This graphitized structure generates extensive hydrophobic domains on the material surface, which enable hydrophobic interactions with the hydrophobic backbones of TKIs (Log $P > 2$, Table S1). Moreover, the aromatic domains of KFB favor π–π stacking with the multiple aromatic rings widely present in TKIs, thereby reinforcing adsorption. In addition, oxygen-containing functionalities not only impart surface wettability but may also provide auxiliary hydrogen bonding or electrostatic sites for interaction with specific functional groups of TKIs.

Overall, KFB combines a porous lamellar structure, high surface area, and mixed hydrophilic–hydrophobic surface chemistry, providing abundant active sites and complementary interaction mechanisms (hydrophobic effect, π–π stacking, and auxiliary hydrogen bonding), collectively enabling efficient extraction of TKIs from plasma.

3.2. Preliminary feasibility evaluation

The studied TKIs exhibit weakly polar properties, with Log P values ranging from 2.93 to 5.81 and pK_a values from 4.62 to 10.07 (Table S1). These parameters indicate strong hydrophobicity, suggesting that their extraction by KFB is primarily driven by hydrophobic interactions, as KFB itself is a hydrophobic material.

Preliminary attempts with a packed-tip format (using degreased cotton as a frit and ~2 mg sorbent) resulted in excessive backpressure, making aspiration and dispensing with a pipettor impractical. This limitation motivated the development of the inner-wall coating strategy. The feasibility of the KFB-tip-based PT-μSPE method for TKI extraction from aqueous media was then assessed by comparing LC-MS/MS chromatograms of a directly injected 500 ng mL^{-1} standard solution and a 100 ng mL^{-1} spiked sample processed *via* the extraction protocol. As shown in Fig. 4A, all TKIs were well separated and

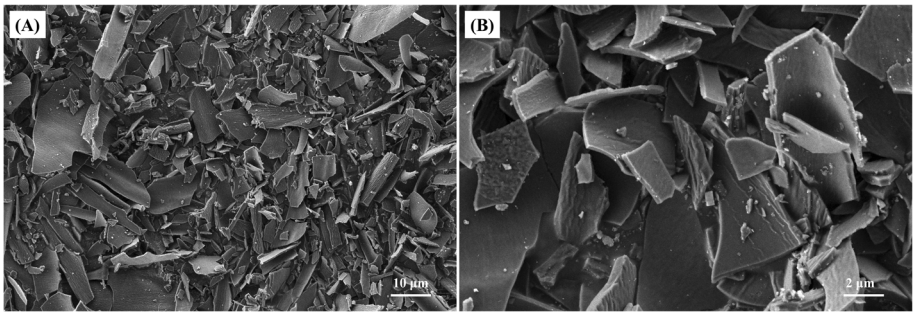

Fig. 2 SEM images of the KFB at different magnifications. (A) 1.00 KX; scale bar: 10 μm. (B) 5.00 KX; scale bar: 2 μm.

Open Access Article. Published on 15 September 2025. Downloaded on 1/19/2026 5:07:36 PM.
This article is licensed under a Creative Commons Attribution-NonCommercial 3.0 Unported Licence.

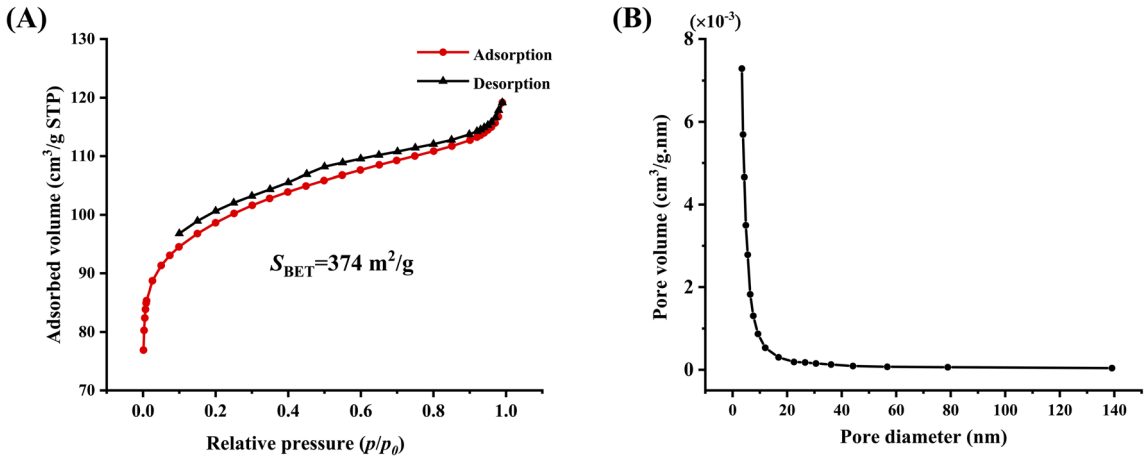

Fig. 3 Nitrogen adsorption–desorption isotherm and BJH pore size distribution of the KFB. (A) N_2 adsorption–desorption isotherm; (B) BJH pore size distribution.

clearly detected in the standard solution. Notably, after extraction, the 100 ng mL^{-1} spiked sample (Fig. 4B) exhibited distinct peaks with signal intensities approaching those of the fivefold higher standard, indicating efficient analyte enrichment by the KFB-tip sorbent. In addition, blank-solution extractions were conducted to evaluate potential interferences from both the HT-902T silicone adhesive and the KFB. The results showed clear baseline with no interfering peaks (data not shown), confirming that the method provided a clean and interference-free background under LC-MS/MS detection in MRM mode. Taken together, these findings demonstrate that the KFB-tip-based PT-μSPE method enables, interference-free effective extraction and enrichment of TKIs from aqueous samples.

The potential influence of the silicone adhesive used to immobilize the KFB was also evaluated. Under the experimental conditions, no material detachment was observed after repeated aspiration/dispensing with EtOH, indicating that the KFB was firmly bound to the pipette tip. Analysis of TKI-free aqueous solutions subjected to the same extraction procedure showed stable baselines with no interference peaks at the retention times and MRM transitions of the TKIs, confirming that their detection was not affected. Moreover, a single-use design was adopted for the KFB-tips to further minimize the risk of leaching or interference in clinical or pharmacokinetic applications.

It is worth noting that although traditional PT-μSPE techniques often require a conditioning step prior to sample loading, preliminary experiments comparing recoveries with and without conditioning revealed no obvious difference (data not shown). Therefore, to streamline the operation and enhance throughput, the conditioning step was omitted in subsequent analyses.

3.3. Optimization of extraction conditions

To optimize the KFB-tip-based PT-μSPE method, a 100 ng mL^{-1} mixed TKI standard solution was employed. Critical variables

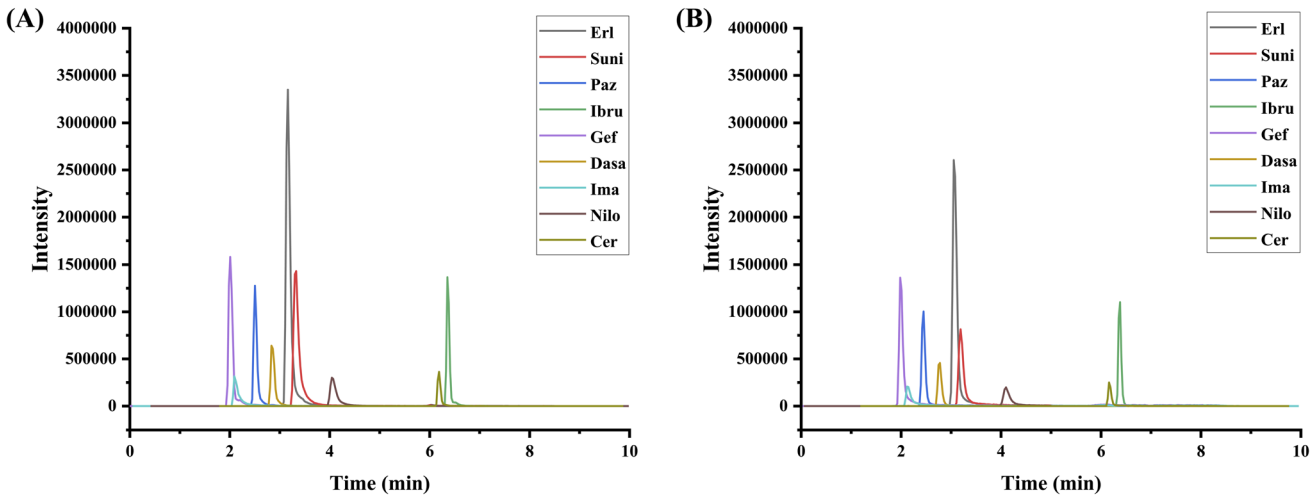

Fig. 4 LC-MS/MS chromatograms of (A) TKI standard solution (500 ng mL^{-1}), and (B) TKI-spiked solution (100 ng mL^{-1}) treated with PT-SPE.

© 2025 The Author(s). Published by the Royal Society of Chemistry

Open Access Article. Published on 15 September 2025. Downloaded on 1/19/2026 5:07:36 PM.
This article is licensed under a Creative Commons Attribution-NonCommercial 3.0 Unported Licence.

such as sample pH, type and volume of the desorption solvent, as well as the number of pipetting cycles for extraction and elution were systematically investigated using a single-factor optimization approach, in which each parameter was varied individually while the others were kept constant. This strategy ensured efficient identification of the most influential conditions while maintaining simplicity and practicality. Extraction efficiency was evaluated by measuring LC-MS/MS peak areas of the target analytes.

3.3.1. pH of sample solution. pH serves as a key factor in modulating both the ionization state of TKIs and their adsorption onto the KFB sorbent. Extraction efficiency was evaluated over a pH range of 3.0 to 11.0. As shown in Fig. 5A, the overall peak areas increased with pH, reaching a maximum at pH 7.0 for most analytes. This suggests that pH 7.0 offers an optimal balance between the analyte's molecular state and the sorbent's adsorption capacity. Therefore, pH 7.0 was selected for subsequent experiments.

3.3.2. Type of desorption solvent. The efficiency of analyte recovery from the KFB sorbent strongly dependent on the choice of desorption solvent. EtOH, MeOH, ACN, and AC were tested as potential desorption solvents. As shown in Fig. 5B, EtOH provided the highest or near-highest peak areas for the majority of TKIs, indicating superior elution capability. This performance can be attributed to its lower polarity and stronger hydrophobicity (dielectric constant ≈ 24.3) compared with Meoh (≈32.6), which enhances its affinity for hydrophobic compounds. Given that the studied TKIs exhibit Log *P* values of 2.93–5.81 (Table S1), their higher solubility in EtOH further facilitates disruption of hydrophobic interactions with the KFB sorbent, leading to more efficient desorption. In addition to its effectiveness, ethanol is less toxic and more environmentally friendly compared to other solvents. Therefore, ethanol was selected as the optimal desorption solvent for subsequent experiments.

3.3.3. Volume of desorption solvent. The volume of desorption solvent directly affects the concentration of analytes in the eluate and thereby impacts detection sensitivity. As illustrated in Fig. 5C, increasing the volume of desorption solvent from 200 to 500 μL resulted in a progressive decline in peak areas for all TKIs, likely due to dilution effects. Among the tested volumes, 200 μL provided the highest signal response, indicating optimal enrichment without compromising desorption efficiency. Therefore, 200 μL was selected as the optimal desorption volume for further experiments.

3.3.4. Number of extraction cycles. The number of aspirating/dispensing cycles during the extraction step determines the contact efficiency between the sorbent and the sample. As illustrated in Fig. 5D, the peak areas of TKIs increased with the number of extraction cycles and reached a plateau around 8 cycles. Beyond this point, further cycles yielded negligible improvement, indicating equilibrium was effectively reached within only a few aspiration/dispensing steps. This rapid approach to equilibrium can be attributed to the thin and uniform sorbent layer formed by the inner-wall coating, which minimizes diffusion distances and facilitates fast mass transfer. Therefore, 8 aspirating/dispensing cycles were selected as optimal for the extraction step.

3.3.5. Number of desorption cycles. Similarly, the effect of aspirating/dispensing repetitions on desorption efficiency was evaluated. As shown in Fig. 5E, peak areas increased with cycle number and stabilized at around 6 cycles for most analytes. Additional cycles offered no significant enhancement, suggesting that 6 cycles are sufficient to fully desorb the analytes. Thus, 6 aspirating/dispensing cycles were adopted for desorption.

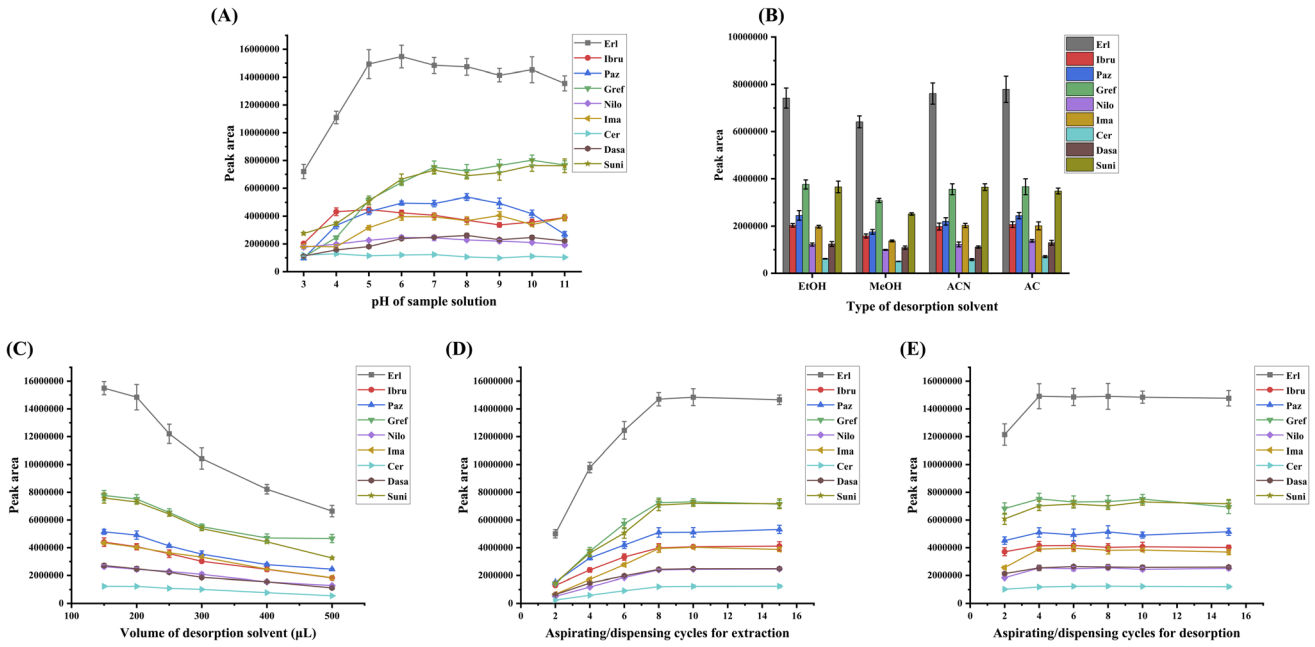

Fig. 5 Optimization of the extraction conditions: (A) pH of sample solution, (B) type of desorption solvent, (C) volume of desorptin solvent, (D) number of aspirating/dispensing cycles of sample solution and (E) number of aspirating/dispensing cycles of desorption solvent.

Open Access Article. Published on 15 September 2025. Downloaded on 1/19/2026 5:07:36 PM.
This article is licensed under a Creative Commons Attribution-NonCommercial 3.0 Unported Licence.

3.4. Reproducibility evaluation

The reproducibility of the KFB-tip was systematically evaluated for the extraction of TKIs. Two sources of variability were considered: (1) different fabrication batches of the KFB-tip using the same kapok fiber, and (2) KFB-tips prepared from four independent batches of raw kapok fiber. As shown in Fig. 6, the KFB-tip demonstrated consistent extraction performance under both conditions. The relative standard deviations (RSDs) of peak areas for the TKIs were within acceptable limits (typically <7.8%) across all four batches in each group, indicating minimal variation attributable to either the raw material source or the fabrication process. Importantly, although the exact amount of sorbent could not be directly controlled, the proposed inner-wall coating strategy—by regulating the adhesive volume (~50 μL) to form a thin and uniform layer—ensured reproducible sorbent distribution, thereby avoiding packing-related variability and backpressure issues while maintaining compatibility with automated pipetting. These results demonstrate that potential differences arising from the source, season, or processing of natural kapok fiber did not noticeably alter the structural framework of the derived biochar, where hydrophobic interactions play the dominant role in analyte adsorption. Overall, these findings confirm the robustness and reliability of the KFB-tip for plasma sample preparation and support its practical applicability in bioanalytical workflows involving LC-MS/MS quantification of TKIs.

3.5. Method validation

Although the proposed method removed most matrix components, residual endogenous substances could still influence ionization efficiency and signal intensity. To address this, an internal standard was introduced for signal correction. Cyproconazole (a triazole fungicide, 10 ng mL^{-1}) was selected because (i) it has a Log *P* value of 2.9 and no dissociation pK_a,[27,28] making it a hydrophobic compound similar to TKIs and suitable for KFB-tip extraction and detection, and (ii) it is a synthetic fungicide widely used in agriculture but absent in human blood, thereby avoiding endogenous interference.

Matrix effects were then evaluated using blank plasma from healthy volunteers spiked with TKIs, which is a standard and widely accepted practice in bioanalytical method validation,[29,30] to assess the impact of plasma matrix components on analyte signal intensity. As shown in Fig. 7 (left panel), the matrix factors (MFs) for the TKIs varied substantially, ranging from approximately 44.8% to 76.2%, indicating different degrees of ion suppression across analytes. To minimize matrix-induced signal variations, internal standards (10 ng mL^{-1}) were used for signal normalization. As illustrated in Fig. 7 (right panel), the internal standard-normalized matrix factors (IS-norm MFs) exhibited markedly improved consistency, with values ranging from 91.6% to 104.7% and visibly reduced variability, as indicated by the shortened error bars. These findings confirm that the use of internal standards effectively compensates for matrix effects and enhances the accuracy of TKI quantification in complex plasma matrices. Accordingly, a quantification method was established based on internal standard calibration and matrix-matched linearity.

Under optimized conditions, the method was validated using plasma samples fortified with known concentrations of TKIs, using an internal standard at 10 ng mL^{-1}. Calibration

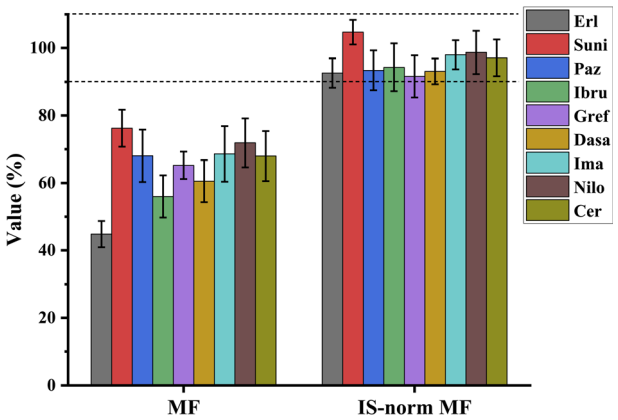

Fig. 7 MF and IS-norm MF for the determination of TKIs using the proposed method ($n = 3$).

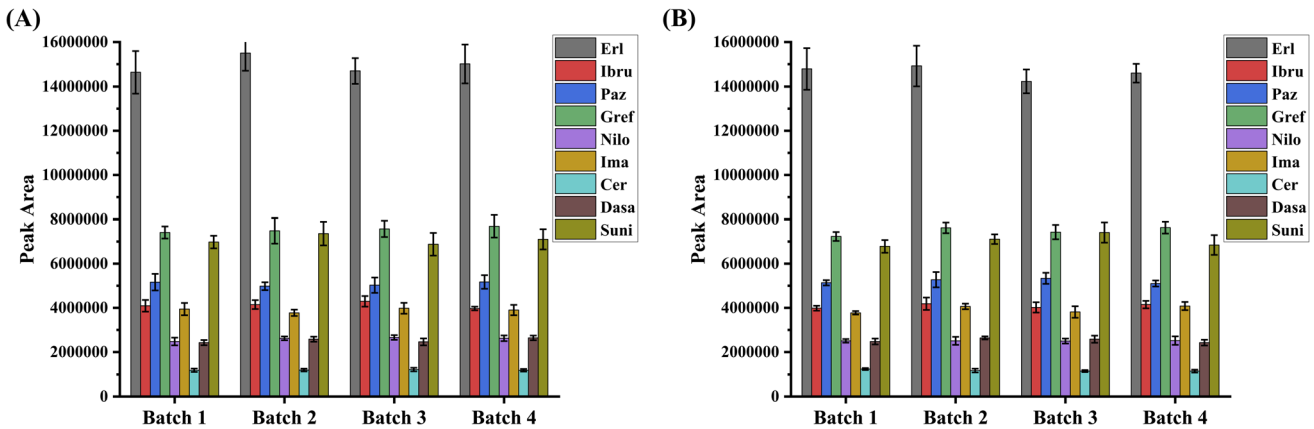

Fig. 6 Peak areas of TKIs using KFB-tips prepared from (A) four fabrication batches and (B) four different kapok fiber sources.

© 2025 The Author(s). Published by the Royal Society of Chemistry

Open Access Article. Published on 15 September 2025. Downloaded on 1/19/2026 5:07:36 PM. This article is licensed under a Creative Commons Attribution-NonCommercial 3.0 Unported Licence.

Table 1 Calibration ranges, regression equations, and LODs for TKIs using the validated KFB-tip-based PT-μSPE coupled with LC-MS/MS

Analyte	Calibration range (ng mL^{-1})	Regression equation	R^2	LOD (ng mL^{-1})
Erl	0.1–200	$y = 2.9057x + 1.4058$	0.9987	0.025
Suni	0.2–200	$y = 1.0594x + 0.7359$	0.9996	0.045
Paz	0.2–200	$y = 0.4705x + 0.2214$	0.9934	0.037
Ibru	0.2–200	$y = 0.4304x + 0.5594$	0.9949	0.041
Gef	0.2–200	$y = 0.3150x + 0.1923$	0.9988	0.060
Dasa	0.1–200	$y = 0.1500x + 0.0448$	0.9999	0.022
Ima	0.5–200	$y = 0.1757x + 0.7430$	0.9958	0.106
Nilo	0.1–200	$y = 0.9651x + 0.6275$	0.9974	0.027
Cer	0.5–200	$y = 0.1373x + 0.0705$	0.9988	0.125

curves were established by plotting the average peak area ratios (analyte/internal standard, $n = 3$) *versus* analyte concentrations, using least-squares linear regression. As summarized in Table 1, the method showed good linearity across the investigated ranges for all TKIs, with correlation coefficients (R^2) exceeding 0.9934. The limits of detection LODs, calculated based on a signal-to-noise ratio (S/N) of 3 : 1, ranged from 0.022 to 0.125 ng mL^{-1}, confirming the method's high sensitivity for trace-level quantification in spiked plasma matrices.

The accuracy and precision of the developed method were evaluated through intra- and inter-day recovery experiments at three concentration levels (low, medium, and high, namely 1, 20, and 100 ng mL^{-1}) using spiked plasma samples. For intra-day assessments, each level was analyzed in triplicate ($n = 3$) within a single day, while inter-day precision was assessed over three consecutive days under the same conditions. As summarized in Table 2, the intra-day recoveries for the TKIs ranged from 85.2% to 111.6%, with corresponding RSDs between 2.8% and 16.1%. Inter-day recoveries ranged from 85.7% to 109.7%, with RSDs between 4.5% and 14.8%. Collectively, these results indicate that the method provides acceptable accuracy and precision across the tested concentration ranges, meeting typical bioanalytical validation requirements for quantitative plasma analysis. Moreover, although high-throughput validation on fully automated platforms (*e.g.*, 96-well robotic systems) was not performed in this study due to equipment limitations, the pipette-tip format and simplified extraction workflow are inherently compatible with standard automated liquid-handling systems, highlighting the strong potential of this method for seamless integration into high-throughput bioanalytical workflows.

3.6. Plasma sample analysis

Ideally, the applicability of a bioanalytical method should be evaluated using real patient plasma samples; however, due to ethical and privacy restrictions, obtaining such samples is challenging. Therefore, to further assess the applicability of the validated quantification method, spiked recovery experiments were performed using human plasma samples fortified with TKIs following a single-blind protocol.[31,32] Specifically, three plasma samples were spiked at randomly selected concentration levels and analyzed without the operator being informed of the target concentrations until the final results were obtained. Upon unblinding, the detected concentrations were expressed as mean ± standard deviation (SD) to reflect the precision of the method. The relative error between the measured and nominal concentrations was calculated to evaluate the method's accuracy.

As summarized in Table 3, the detected concentrations across three independently spiked plasma samples

Table 2 Intra-day and inter-day recoveries and RSDs at low, medium, and high concentration levels (1, 20, and 100 ng mL^{-1}) obtained using the validated KFB-tip-based PT-μSPE coupled with LC-MS/MS for TKI analysis ($n = 3$)

	Intra-day						Inter-day					
	Low		Medium		High		Low		Medium		High	
Analyte	Recovery (%)	RSD (%)	Recovery (%)	RSD (%)	Recovery (%)	RSD (%)	Recovery (%)	RSD (%)	Recovery (%)	RSD (%)	Recovery (%)	RSD (%)
Erl	100.6	11.0	85.7	9.8	85.2	8.3	97.7	8.2	87.7	11.4	85.7	13.7
Suni	95.9	12.1	94.2	4.6	93.9	7.5	97.1	11.1	94.2	6.0	98.7	5.0
Paz	102.2	16.1	102.5	7.4	96.4	5.2	100.1	14.8	100.5	9.7	97.6	4.5
Ibru	87.0	10.0	93.5	7.2	97.6	10.7	85.7	13.7	93.1	7.8	101.3	6.9
Gef	108.0	13.3	107.5	11.5	100.4	13.6	109.7	14.7	103.4	8.0	100.2	10.6
Dasa	113.9	5.6	101.3	5.1	87.3	10.2	105.9	10.3	95.0	10.6	87.1	14.7
Ima	86.2	7.1	97.6	13.8	101.2	12.1	90.7	10.5	89.9	12.3	101.3	6.5
Nilo	97.3	13.2	111.6	7.6	100.7	5.4	92.3	14.7	107.4	14.8	94.9	4.5
Cer	91.8	12.7	86.7	14.8	95.2	4.0	106.2	10.6	90.7	11.7	94.5	10.9

Open Access Article. Published on 15 September 2025. Downloaded on 1/19/2026 5:07:36 PM. This article is licensed under a Creative Commons Attribution-NonCommercial 3.0 Unported Licence.

Table 3 Spiked and detected concentrations of TKIs in plasma (mean ± SD, $n = 3$) at randomly selected spiking levels, including relative errors, as analyzed by the validated method

	Plasma 1 (spiked level: 2.6 ng mL^{-1})		Plasma 2 (spiked level: 18.5 ng mL^{-1})		Plasma 3 (spiked level: 168.0 ng mL^{-1})	
Analyte	Detected level (mean ± SD, ng mL^{-1})	Relative error (%)	Detected level (mean ± SD, ng mL^{-1})	Relative error (%)	Detected level (mean ± SD, ng mL^{-1})	Relative error (%)
Erl	2.63 ± 0.18	1.20	19.32 ± 0.96	4.4	159.02 ± 4.42	−5.3
Suni	2.46 ± 0.09	−5.40	18.91 ± 1.05	2.2	155.15 ± 10.63	−7.6
Paz	2.64 ± 0.22	1.50	17.59 ± 0.51	−4.9	163.25 ± 7.55	−2.8
Ibru	2.57 ± 0.20	−1.20	18.94 ± 0.51	2.4	162.90 ± 6.24	−3.0
Gef	2.42 ± 0.15	−6.90	17.65 ± 0.81	−4.6	171.48 ± 3.83	2.1
Dasa	2.44 ± 0.08	−6.20	17.22 ± 1.16	−6.9	182.14 ± 11.00	8.4
Ima	2.66 ± 0.17	2.30	19.17 ± 0.81	3.6	158.05 ± 7.07	−5.9
Nilo	2.49 ± 0.18	−4.20	17.83 ± 0.95	−3.6	163.46 ± 7.52	−2.7
Cer	2.51 ± 0.12	−3.50	20.07 ± 1.18	8.5	181.39 ± 11.74	8.0

demonstrated excellent agreement with the theoretical values, with relative errors ranging from −7.6% to +8.5%. These deviations are well within acceptable limits for quantitative bioanalysis, indicating high trueness of the method. Moreover, the calculated RSDs of the detected concentrations were all below 8.3%, reflecting satisfactory repeatability and precision under real sample conditions. The consistent recoveries across different TKIs and plasma replicates highlight the robustness of the KFB-tip-based extraction strategy in complex biological matrices. Collectively, the results demonstrate that the proposed method enables reliable quantification of TKIs in plasma and shows strong potential for application in therapeutic drug monitoring and pharmacokinetic studies.

3.7. Method's greenness evaluation

The greenness of the developed method was evaluated using five complementary metrics: GAPI (Green Analytical Procedure Index), AGREE (Analytical GREEnness Metric), AGREEprep (Analytical Greenness Metric for Sample Preparation), SPMS (Sample Preparation Metric of Sustainability), and BAGI (Biological Analytical Green Index), which together assess environmental impact across procedural, preparative, and biological dimensions of green analytical chemistry.

GAPI employs a pentagonal pictogram divided into 15 segments, each representing a key aspect of the analytical process, including sampling, transport, storage, preparation, and final determination.[33,34] Each segment is color-coded to reflect its environmental impact: green (low impact), yellow (medium impact), or red (high impact). As depicted in Fig. 8A, the evaluated method achieved eight green, three yellow, and four red segments, indicating a generally good overall greenness despite some high-impact areas. The four red segments were mainly associated with off-line plasma collection, transport and storage requirements, the need for extraction, and energy/waste management. These deductions largely reflect the intrinsic features of bioanalytical workflows (*e.g.*, unavoidable off-line sampling and transport in therapeutic drug monitoring), rather than drawbacks of the proposed method itself.

AGREE, presented as a circular diagram, evaluates an analytical method's greenness based on 12 principles of green analytical chemistry.[35] Each of its 12 segments is color-coded (green, yellow, red) to indicate adherence to a principle, signifying low, medium, or high environmental impact, respectively. A central numerical score, ranging from 0 to 1, provides an overall greenness assessment. As depicted in Fig. 8B, the AGREE diagram for this method displayed a central score of 0.76, surpassing the 0.6 threshold, which suggests a good level of greenness and indicates that the method largely adheres to green chemistry principles.

AGREEprep, a specialized variant of the AGREE metric for sample preparation, is presented as a circular diagram, typically with 10 segments representing different greenness aspects of this crucial step.[36] Similar to AGREE, it uses color-coding (green, yellow, orange/red) to visually represent the environmental impact for each aspect. A central numerical score provides an aggregated greenness assessment specifically for the sample preparation procedure. As depicted in Fig. 8C, the current method's sample preparation score of 0.64, slightly above the 0.6 threshold, indicating a moderate level of greenness and highlighting areas for further improvement. The deductions mainly arose from criteria not yet fully satisfied, such as in-line automation and high-throughput capability, as well as necessary penalties associated with solvent use. These limitations could be overcome in future adaptations by applying the pipette-tip format to automated liquid-handling systems or multi-channel pipettors, enabling in-line processing and higher throughput, thereby improving AGREEprep performance.

The SPMS tool provides a block-based visual evaluation of sample preparation methods.[37] It categorizes different aspects such as "Sample", "Extractant", "Energy & Waste", and "Procedure" into distinct, variably sized blocks. The greenness within these categories is indicated by internal color coding (*e.g.*, green for favorable, orange for less favorable). For SPMS, scores range from 0 to 10, with values above 6.0 typically indicating a "green" sample preparation method. As shown in Fig. 8D, the current method's central numerical score of 7.68 offers an overall assessment of the sample preparation method's performance across these multiple criteria, with this score confirming that the protocol is considered "green".

BAGI, more accurately described as the Blue Applicability Grade Index, evaluates the practicality of an analytical method

 © 2025 The Author(s). Published by the Royal Society of Chemistry

Open Access Article. Published on 15 September 2025. Downloaded on 1/19/2026 5:07:36 PM.
This article is licensed under a Creative Commons Attribution-NonCommercial 3.0 Unported Licence.

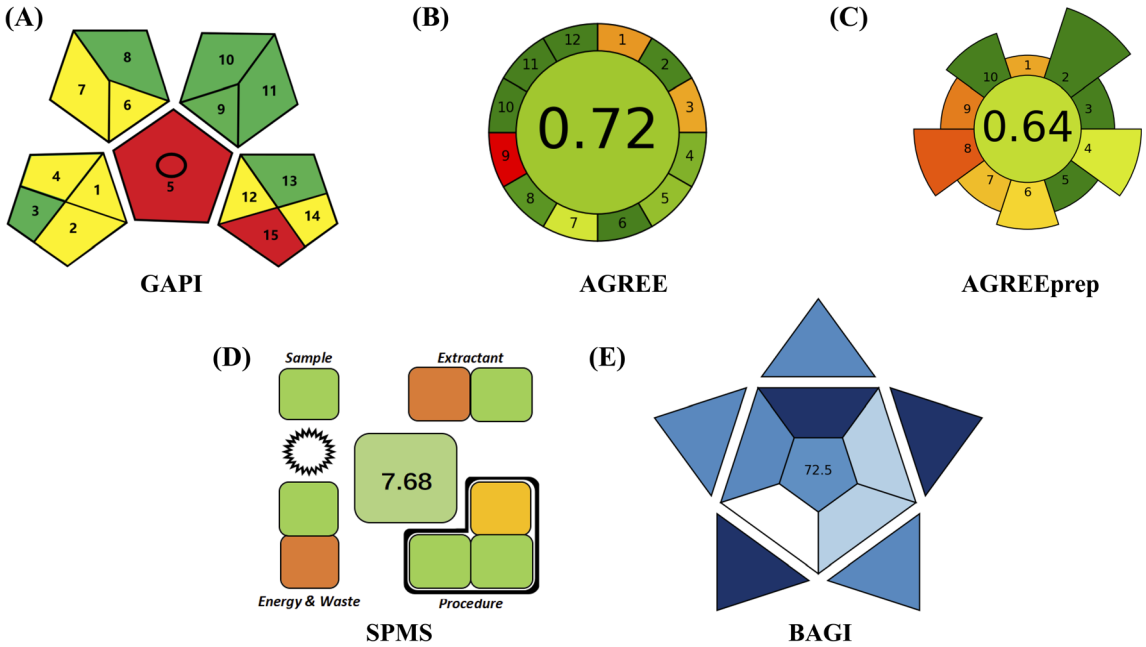

Fig. 8 Greenness assessment of the developed method using five widely recognized green analytical chemistry metrics: (A) GAPI, (B) AGREE, (C) AGREEprep, (D) SPMS, and (E) BAGI.

rather than its environmental greenness.[38] Its score ranges from 25 to 100, where higher values indicate greater practicality and applicability. Specific points (10, 7.5, 5.0, 2.5) correspond to different hues of blue (dark blue to white), visually representing the level of practicality for various attributes. As shown in Fig. 8E, the method, with a BAGI score of 72.5, signifies a good level of practicality and applicability.

Overall, the comprehensive evaluation using these green analytical chemistry tools demonstrates that the developed method exhibits a generally good level of greenness. While the AGREE and SPMS scores indicate strong adherence to green principles, the GAPI and AGREEprep analyses highlight specific areas—particularly off-line sampling, transport, and automation—where further optimization could enhance the method's environmental profile.

3.8. Method comparison

The analytical performance of the proposed KFB-PT-μSPE method, in terms of plasma volume requirement and detection sensitivity (LOD: 0.022–0.125 ng mL^{-1}), is comparable to or even superior to those of previously reported LC-MS/MS methods for TKIs (Table 4). For instance, traditional μ-SPE using PRiME sorbents required 300 μL plasma and 500 μL MeOH, yielding higher LODs (0.30–5.03 ng mL^{-1}). Similarly, MSPE methods employing HLB magnetic particles consumed larger solvent volumes (up to 750 μL MeOH/ACN) and provided LODs of 2.5–10.0 ng mL^{-1}. Even advanced materials such as polydopamine–graphene oxide or molecularly imprinted polymers showed LODs in the 0.35–5.8 ng mL^{-1} range, while often relying on milliliter-level organic solvents. Compared with these methods, the present protocol achieves lower LODs with only 100 μL plasma and 200 μL EtOH, representing both high analytical sensitivity and reduced sample/solvent demand.

Beyond sensitivity and volume efficiency, several practical advantages are also evident: (1) unlike many existing protocols that require protein precipitation prior to extraction and solvent evaporation followed by reconstitution before LC-MS/MS analysis, the present method eliminates both steps. Plasma samples can be directly subjected to extraction, and the ethanol eluate can be injected without further processing, significantly streamlining the sample preparation procedure. (2) The use of kapok fiber-derived biochar as the sorbent and EtOH for desorption results in a highly eco-friendly protocol. Both materials are biodegradable, non-toxic, and inexpensive, aligning well with the principles of green analytical chemistry. (3) The unique inner-wall coating design results in a hollow-tip configuration with minimal backpressure, enabling seamless integration with semi-automated electronic pipettes. This feature also lays the foundation for full automation by coupling with robotic liquid handling systems, facilitating high-throughput LC-MS/MS analysis in clinical or pharmacokinetic settings. Overall, the developed method not only ensures reliable quantification of TKIs in plasma but also achieves notable improvements in operational simplicity, environmental sustainability, and automation potential.

At the same time, some limitations should be acknowledged. The current method still relies on off-line plasma collection and transportation, which may limit its greenness profile as reflected in the GAPI assessment. Moreover, although semi-automation has been demonstrated, full integration with liquid-handling workstations should be pursued to realize its high-throughput potential in routine clinical applications. Finally, while the method has been validated in plasma, its

Open Access Article. Published on 15 September 2025. Downloaded on 1/19/2026 5:07:36 PM.
This article is licensed under a Creative Commons Attribution-NonCommercial 3.0 Unported Licence.

Table 4 Comparison of the proposed method with previously reported LC-MS/MS methods for the determination of TKIs

Sample	Analyte	Sample preparation method	Sorbent	Organic solvent usage	Instrument detection	LOD	Ref.
Plasma (300 μL)	Baricitinib, Bosutinib, Dasa, Filgotinib, Ima, Ibru, Nilo, Peficitinib, Ponatinib, Ruxolitinib, Tofacitinib	μSPE	PRiME μ-SPE MCX	500 μL MeOH	LC-MS/MS	0.30–5.03 ng mL^{-1}	39
Plasma (100 μL)	Afa, Alectinib, Apatinib, Cer, Criz, Dasa, Erl, Gef, Icotinib, Ima, Lapatinib, *N*-desmethyl imatinib, Regorafenib, Sorafenib, Vemurafenib	MSPE	HLB magnetic particles	150 μL MeOH and 600 μL ACN	LC-MS/MS	2.5–10.0 ng mL^{-1}	40
Plasma (100 μL)	Erl, Ibru, Paz, Afatinib, Gef, Nilo, Ima, Crizotinib, Cer, Suni, Dasa	IS-SPE	Polypropylene nonwoven	200 μL ACN	LC-MS/MS	0.02–0.14 ng mL^{-1}	11
Plasma (100 μL)	Alectinib and its active metabolite	PT-SPE	Porous polydopamine graphene oxide	200 μL ACN, 1.94 mL MeOH and 0.36 mL triethylamine	LC-UV	3.9–4.8 ng mL^{-1}	41
Plasma (200 μL)	Ima, Dasa, Nilo, Ponatinib	Thin-film microextraction	Molecularly imprinted polymer	200 μL ACN	LC-MS/MS	0.5–5.8 ng mL^{-1}	42
Plasma (2000 μL)	Suni	Dispersive solid phase extraction	MIL-101Cr (NH_2)@SiO_2@$NiFe_2O_4$	1 mL ACN and 100 μL DMF	LC-MS/MS	0.35 ng mL^{-1}	43
Plasma (100 μL)	Erl, Suni, Paz, Ibru, Gef, Dasa, Ima, Nilo, Cer	PT-μSPE	KFB	200 μL EtOH	LC-MS/MS	0.022–0.125 ng mL^{-1}	Current work

© 2025 The Author(s). Published by the Royal Society of Chemistry

Open Access Article. Published on 15 September 2025. Downloaded on 1/19/2026 5:07:36 PM. This article is licensed under a Creative Commons Attribution-NonCommercial 3.0 Unported Licence.

applicability to other complex biological matrices (*e.g.*, urine, saliva, cerebrospinal fluid) remains to be explored. Addressing these aspects in future work will further enhance both the practicality and environmental sustainability of the proposed approach.

4. Conclusion

The KFB-based PT-μSPE method presented in this study offers a highly efficient, cost-effective, and environmentally sustainable approach for the extraction and quantification of TKIs in plasma. By integrating green biochar materials with automated pipette-tip extraction, the method effectively minimizes solvent consumption and simplifies sample preparation while maintaining excellent extraction efficiency, low LOD (0.022 to 0.125 ng mL^{-1}), robust reproducibility, and minimal matrix interference. Its unique design ensures compatibility with semi-automated pipettes and future robotic liquid-handling platforms, supporting high-throughput LC-MS/MS analysis in clinical and pharmacokinetic applications. Nevertheless, some limitations should be acknowledged, including reliance on off-line plasma collection and transport, partial (rather than full) automation, and validation restricted to plasma. Future studies should therefore focus on achieving complete integration with automated liquid-handling stations, extending validation to other complex biological matrices (*e.g.*, urine, saliva, cerebrospinal fluid), and further optimizing biochar sorbent properties. Addressing these aspects will enhance the practicality, versatility, and environmental sustainability of the method, reinforcing its potential as a powerful tool for therapeutic drug monitoring and personalized medicine.

Author contributions

Xiaofei Zhang: methodology, data curation, writing – original draft, resources. Mengyuan Lv: methodology, writing – original draft. Yuyang Wang: methodology, writing – original draft. Nan Zhang: supervision, writing – review & editing. Di Chen: project administration, conceptualization, funding acquisition, writing – review & editing.

Conflicts of interest

The authors declare that they have no competing interests.

Data availability

All data underlying the results are available as part of the article and no additional source data is required.

Supplementary information is available. The SI includes detailed molecular information and chemical structures of the studied TKIs (Table S1), their mass spectrometric parameters (Table S2), and supporting figures: schematic illustration of KFB preparation (Fig. S1), fabrication process and photograph of the KFB-tip device (Fig. S2), schematic assembly of the KFB-tip extraction unit (Fig. S3), FT-IR spectrum of KFB (Fig. S4), and XPS spectra of KFB (Fig. S5). See DOI: **https://doi.org/10.1039/d5ra05405b**.

Acknowledgements

This work was supported by the National Natural Science Foundation of China (8240081392) and the Wu Jieping Medical Foundation (320.6750.2024-20-10).

References

1 L. Huang, S. Jiang and Y. Shi, *J. Hematol. Oncol.*, 2020, **13**, 143.
2 A. Shinde, K. Panchal, S. Katke, R. Paliwal and A. Chaurasiya, *Therapies*, 2022, **77**, 425–443.
3 J. N. Henriksen, C. U. Andersen and N. Fristrup, *Clin. Genitourin. Cancer*, 2024, **22**, 102064.
4 A. Mueller-Schoell, S. L. Groenland, O. Scherf-Clavel, M. Van Dyk, W. Huisinga, R. Michelet, U. Jaehde, N. Steeghs, A. D. R. Huitema and C. Kloft, *Eur. J. Clin. Pharmacol.*, 2021, **77**, 441–464.
5 S. Noda, D. Hira, R. Osaki, T. Fujimoto, H. Iida, S. Tanaka-Mizuno, A. Andoh, M. Tani, Y. Ikeda, S.-Y. Morita and T. Terada, *Cancer Chemother. Pharmacol.*, 2020, **86**, 129–139.
6 Z. He, X. Zhou, Z. Wen, Z. Gao, H. Chen, Q. Wang, H. Liang, D. Luo, X. Liu, N. Xu and Q. Liu, *Blood*, 2023, **142**, 1807.
7 Z. He, Q. Zhang, X. Zhou, Q. Wang, X. Liu and N. Xu, *Blood*, 2024, **144**, 1773.
8 J. Ye, M. Bi, H. Yao, D. Yang and D. Chen, *Microchem. J.*, 2024, **201**, 110694.
9 S. N. Thomas, D. French, P. J. Jannetto, B. A. Rappold and W. A. Clarke, *Nat. Rev. Methods Primers*, 2022, **2**, 96.
10 L. Chen, Y. Zhang, Y.-X. Zhang, W.-L. Wang, D.-M. Sun, P.-Y. Li, X.-S. Feng and Y. Tan, *J. Pharm. Anal.*, 2024, **14**, 100899.
11 J. Ye, Y. Zheng, X. Li, X. Jiang and D. Chen, *Anal. Chim. Acta*, 2024, **1329**, 343240.
12 H. Sun, J. Feng, S. Han, X. Ji, C. Li, J. Feng and M. Sun, *Microchim. Acta*, 2021, **188**, 189.
13 Q. Li, B. Deng, R. Feng, D. Chen and L. Hua, *Sustain. Chem. Pharm.*, 2025, **43**, 101906.
14 Z. Huang, P. Liu, H. Chen, X. Lin, Y. Zhou, Y. Xing and H. K. Lee, *J. Hazard. Mater.*, 2023, **448**, 130955.
15 Z. Yan, B. Hu, Q. Li, S. Zhang, J. Pang and C. Wu, *J. Chromatogr. A*, 2019, **1584**, 33–41.
16 Q. Jiang, S. Zhang and M. Sun, *TrAC, Trends Anal. Chem.*, 2023, **168**, 117283.
17 Y. Chen, Y. Qi, Q. Li, C. Xiao, H. Chen and X. Dang, *Microchem. J.*, 2024, **207**, 112112.
18 Y. Liu, X. Dang and H. Chen, *Anal. Chim. Acta*, 2023, **1273**, 341493.
19 W. A. Khan, M. B. Arain, S. Balal, A. Niaz, A. Mollahosseini and M. Soylak, *J. Sep. Sci.*, 2025, **48**, e70074.
20 R. Sun, F. Lu, C. Yu, Y. Yang, L. Qiao and A. Liu, *J. Chromatogr. A*, 2022, **1673**, 463101.
21 N. Torres-Lara, A. Molina-Balmaceda, D. Arismendi and P. Richter, *Green Anal. Chem.*, 2023, **6**, 100073.

© 2025 The Author(s). Published by the Royal Society of Chemistry

Open Access Article. Published on 15 September 2025. Downloaded on 1/19/2026 5:07:36 PM.
This article is licensed under a Creative Commons Attribution-NonCommercial 3.0 Unported Licence.

22 C. D. S. Cardoso, M. Pereira-Coelho, F. L. Faita and L. Vitali, *Green Anal. Chem.*, 2025, **13**, 100251.
23 A. Keikavousi Behbahan, V. Mahdavi, Z. Roustaei and H. Bagheri, *Food Chem.*, 2021, **360**, 130085.
24 Y. Liu, W. Li, Y. Zheng, B. Deng, L. Ma and D. Chen, *Sustain. Chem. Pharm.*, 2024, **40**, 101640.
25 Y. Zheng, J. Wang, Y. Zhu and A. Wang, *J. Environ. Sci.*, 2015, **27**, 21–32.
26 Z. Yang, F. Li, F. Guan, F. Wang, C. Wang and Y. Qiu, *Cellulose*, 2023, **30**, 789–799.
27 J. A. Ferreira, A. C. Fassoni, J. M. S. Ferreira, P. M. P. Lins and C. B. G. Bottoli, *Horticulturae*, 2022, **8**, 1099.
28 W. A. Wan Ibrahim, D. Hermawan, M. N. Hasan, H. Y. Aboul Enein and M. M. Sanagi, *Chromatographia*, 2008, **68**, 415–419.
29 F. Raposo and D. Barceló, *TrAC, Trends Anal. Chem.*, 2021, **134**, 116068.
30 A. Nasiri, R. Jahani, S. Mokhtari, H. Yazdanpanah, B. Daraei, M. Faizi and F. Kobarfard, *Analyst*, 2021, **146**, 6049–6063.
31 M. Siebenhaar, K. Küllmer, N. M. De Barros Fernandes, V. Hüllen and C. Hopf, *Anal. Bioanal. Chem.*, 2015, **407**, 7229–7238.
32 J. Millán-Santiago, R. Lucena and S. Cárdenas, *Anal. Bioanal. Chem.*, 2022, **414**, 5287–5296.
33 J. Płotka-Wasylka, *Talanta*, 2018, **181**, 204–209.
34 J. Płotka-Wasylka and W. Wojnowski, *Green Chem.*, 2021, **23**, 8657–8665.
35 F. Pena-Pereira, W. Wojnowski and M. Tobiszewski, *Anal. Chem.*, 2020, **92**, 10076–10082.
36 W. Wojnowski, M. Tobiszewski, F. Pena-Pereira and E. Psillakis, *TrAC, Trends Anal. Chem.*, 2022, **149**, 116553.
37 R. González-Martín, A. Gutiérrez-Serpa, V. Pino and M. Sajid, *J. Chromatogr. A*, 2023, **1707**, 464291.
38 N. Manousi, W. Wojnowski, J. Płotka-Wasylka and V. Samanidou, *Green Chem.*, 2023, **25**, 7598–7604.
39 D. Koller, V. Vaitsekhovich, C. Mba, J. L. Steegmann, P. Zubiaur, F. Abad-Santos and A. Wojnicz, *Talanta*, 2020, **208**, 120450.
40 G. Li, M. Zhao and L. Zhao, *J. Pharm. Biomed. Anal.*, 2022, **212**, 114517.
41 P. Zhang, W. Wang, J. Yin, M. Wang, Y. Han and H. Yan, *J. Chromatogr. A*, 2024, **1714**, 464578.
42 E. Langille, K. A. Hanrahan and C. S. Bottaro, *Talanta Open*, 2023, **8**, 100240.
43 M. Hassani Nouriyeh, M. R. Afshar Mogaddam, M. Nemati, M. A. Farajzadeh, A. Abbasalizadeh and A. Shahedi Hojghan, *J. Chromatogr. B*, 2024, **1239**, 124109.

© 2025 The Author(s). Published by the Royal Society of Chemistry